

Impact of insulin deprivation and treatment on sphingolipid distribution in different muscle subcellular compartments of streptozotocin-diabetic C57Bl/6 mice

Piotr Zabielski, Agnieszka Blachnio-Zabielska, Ian R. Lanza, Srinivas Gopala, S. Manjunatha, Daniel R. Jakaitis, Xuan-Mai Persson, Jaime Gransee, Katherine A. Klaus, Jill M. Schimke, Michael D. Jensen, and K. Sreekumaran Nair

Division of Endocrinology and Metabolism, Mayo Clinic College of Medicine, Rochester, Minnesota

Submitted 5 December 2012; accepted in final form 18 December 2013

Zabielski P, Blachnio-Zabielska A, Lanza IR, Gopala S, Manjunatha S, Jakaitis DR, Persson X, Gransee J, Klaus KA, Schimke JM, Jensen MD, Nair KS. Impact of insulin deprivation and treatment on sphingolipid distribution in different muscle subcellular compartments of streptozotocin-diabetic C57Bl/6 mice. *Am J Physiol Endocrinol Metab* 306: E529–E542, 2014. First published December 24, 2013; doi:10.1152/ajpendo.00610.2012.—Insulin deprivation in type 1 diabetes (T1D) individuals increases lipolysis and plasma free fatty acids (FFA) concentration, which can stimulate synthesis of intramyocellular bioactive lipids such as ceramides (Cer) and long-chain fatty acid-CoAs (LCFa-CoAs). Ceramide was shown to decrease muscle insulin sensitivity, and at mitochondrial levels it stimulates reactive oxygen species production. Here, we show that insulin deprivation in streptozotocin diabetic C57Bl/6 mice increases quadriceps muscle Cer content, which was correlated with a concomitant decrease in the body fat and increased plasma FFA, glycosylated hemoglobin level (%Hb A_{1c}), and muscular LCFa-CoA content. The alternations were accompanied by an increase in protein expression in LCFa-CoA and Cer synthesis (FATP1/ACSVL5, CerS1, CerS5), a decrease in the expression of genes implicated in muscle insulin sensitivity (GLUT4, GYS1), and inhibition of insulin signaling cascade by Akt α and GYS3 β phosphorylation under acute insulin stimulation. Both the content and composition of sarcoplasmic fraction sphingolipids were most affected by insulin deprivation, whereas mitochondrial fraction sphingolipids remained stable. The observed effects of insulin deprivation were reversed, except for content and composition of LCFa-CoA, CerS protein expression, GYS1 gene expression, and phosphorylation status of Akt and GYS3 β when exogenous insulin was provided by subcutaneous insulin implants. Principal component analysis and Pearson's correlation analysis revealed close relationships between the features of the diabetic phenotype, the content of LCFa-CoAs and Cers containing C18-fatty acids in sarcoplasm, but not in mitochondria. Insulin replacement did not completely rescue the phenotype, especially regarding the content of LCFa-CoA, or proteins implicated in Cer synthesis and muscle insulin sensitivity. These persistent changes might contribute to muscle insulin resistance observed in T1D individuals.

type 1 diabetes; skeletal muscle; mitochondria; ceramide; long-chain fatty acid-coenzyme A

METICULOUS GLYCEMIC CONTROL in type 1 diabetic (T1D) individuals can be achieved by administration of prandial, short-acting, and long-acting insulin to mimic β -cell secretion in response to varying nutrient levels. Metabolic control in these individuals and stringent adherence to guidelines normalize the

plasma glucose and glycosylated hemoglobin levels (%Hb A_{1c}) and allow for relatively normal life in T1D. Yet T1D individuals are at greater risk of developing cardiovascular disorders and also known to develop insulin resistance (12, 17). The molecular mechanisms responsible for insulin resistance in T1D subjects are unclear, but variable glucose concentrations (28, 70), advanced glycation end products (62, 73), or desensitization of target tissues by insulin (61) have been proposed. Subcutaneous insulin delivery using an insulin pump partially mimics β -cell insulin secretion. However, unlike in nondiabetic individuals with twofold higher hepatic insulin concentration than in the peripheral circulation, the diabetic individuals and animals receiving insulin via subcutaneous pump have similar systemic insulin levels as in liver. Although subcutaneous insulin administration suppresses hepatic gluconeogenesis, decreases protein degradation, and inhibits adipose tissue lipolysis, the lack of adequate insulin effect on triacylglycerol stores leads to the increase in free fatty acids (FFA) in the plasma of T1D individuals via the activation of hormone-sensitive lipase (32). The high FFA in plasma in turn can stimulate lipid accumulation in skeletal muscle, which is associated with insulin resistance (34, 40). Accumulation of intramyocellular ceramides (65, 66) and diacylglycerols (2, 31, 48) and their immediate precursors long-chain fatty acid-acyl-coenzyme A (LCFa-CoA) (3, 21) are associated with decreased muscle glucose disposal and reduced insulin sensitivity in adults with type 2 diabetes (T2D). Because ceramide accumulation, especially palmitoyl-ceramide (C16-Cer), can induce insulin resistance in vivo (37, 71) and in vitro (53, 59), these molecules have become prime suspects in pathogenesis of muscle insulin resistance in type 2 diabetes. However, not much is known about muscle sphingolipid content and composition in T1D. Intramyocellular accumulation of ceramide was observed in the streptozotocin (STZ)-diabetic rat model (8), muscle-specific insulin receptor knockout mice, and STZ-treated mice (23). Thus, insulin deprivation or hypoinsulinemia leads to ceramide accumulation, but it has never been shown whether insulin treatment reverses the accumulation of ceramides in muscle. First, an experiment in which insulin treatment is withdrawn is important to clearly demonstrate the effect of insulin deprivation on ceramides. Long-chain hydrophobic ceramides are impermeable to the cellular membranes (4) and do not move freely between cellular compartments. This feature of long-chain ceramides underscores importance of evaluating distinct pools of ceramides found in plasma membranes, sarcoplasmic reticulum, or mitochondria, which can be regulated differently (7). Additionally, alternation in

Address for reprint requests and other correspondence: K. S. Nair, Div. of Endocrinology and Metabolism, Mayo Clinic College of Medicine, 200 First St. SW, Rochester, MN 55905 (e-mail: nair@mayo.edu).

sphingolipid content at the level of endoplasmic reticulum (ER) can trigger ER stress response (54), whereas at the level of mitochondria it can impair mitochondrial metabolism and stimulate reactive species production (24, 76). Both processes are known to impair insulin sensitivity of target tissues. Thus it is important to evaluate sphingolipid composition of different cellular fractions.

Both plasma and intramuscular lipids with different acyl chain length and unsaturation (double bond no.) have distinctive impacts on muscle insulin sensitivity (14, 19), pancreatic insulin secretion (63, 75), and induction of metabolic disturbances. High content of long-chain saturated fatty acids compared with their unsaturated counterparts [low unsaturation index (UI)] in the Western-type diet is considered to be a major cause of both the obesity and muscle insulin resistance (13, 18). Although individual fatty acid composition of ceramides was studied in detail in animal models of T2D (50) and insulin-resistant human subjects (20), none of the studies addressed T1D models. Recent studies show that not only saturated fats (SAT) but also their monounsaturated species (MUFA) are detrimental for whole body glucose disposal (30) and can lead to insulin resistance (46) and that intramyocellular triglyceride unsaturation index and MUFA content positively correlate with estimation of insulin resistance (27). Thus it is important to evaluate not only intramuscular lipid content but also composition at the level of individual lipid species for both insulin-deprived and -treated states.

Therefore, the objective of the current investigation was to assess the impact of streptozotocin diabetes on the plasma FFA, muscle tissue LCFa-CoA and Cer, and the muscle expression of proteins implicated in lipid synthesis and insulin sensitivity in mice. To determine the degree by which insulin treatment can reverse the effects of insulin deprivation, we used long-lasting subcutaneous insulin implants to normalize diabetic phenotype in STZ T1D animals.

MATERIALS AND METHODS

Animal model. Experiments were conducted using 13-wk-old male C57BL/6J mice (Jackson Laboratory, Bar Harbor, ME). Mice were housed individually with free access to water and chow (TD.10112; Harlan Laboratories, Indianapolis, IN), with a 12:12-h light-dark cycle and temperature and humidity control. Mice were acclimated for 1 wk prior to the beginning of the experiment. The protocol was approved by the Mayo Clinic Institutional Animal Care and Use Committee. Following a 6-h fast, mice were given intraperitoneal injections of STZ (125 mg/kg; in sodium acetate buffer, pH = 4.5) (67). Injections were repeated on the following day. Control animals received intraperitoneal injection of vehicle. Only mice that displayed blood glucose ≥ 300 mg/dl and an increase in blood ketones (both values by Precision Xtra glucometer; Abbott Laboratories, Abbott Park, IL), hyperphagia, and polyuria and were positive for urine glucose presence via dipstick (Uristix, Bayer, Pittsburgh, PA) on *day 7* after the first STZ dose were included in the experiment. Animals that were positive for STZ diabetes received LinBit subcutaneous insulin implant (LinShin Canada, Toronto, ON, Canada) (79) under pentobarbital sodium anesthesia (Nebutal, 40 mg/kg of body wt) according to the manufacturer's protocol. Each animal received two subcutaneous implants (total dose: 0.2 U/24 h for >30 days, 10 U/kg for 20-g mice). Insulin treatment was continued for 3 wk. Control animals (C; $n = 13$) received blank implants. Diabetic control was confirmed by biweekly measurements of blood and urinary glucose. In some cases, when urine glucose was present and blood glucose was >288 mg/dl, the animal received a third implant. The insulin treatment was continued until initially lower plasma glucose content in diabetic animals reached control values. Three weeks following implantation, diabetic mice were divided randomly into diabetic-treated (D + I; $n = 13$) and diabetic-deprived (D - I; $n = 13$) groups. Insulin implants were removed from the D - I group under pentobarbital anesthesia, which led to the return of the diabetic phenotype within 24 h. Animals from the D + I group continued on insulin treatment (Fig. 1). At the age of 18 wk, animals from all groups were analyzed for body composition by an Echo-MRI Body Composition Analyzer (EchoMRI, Houston, TX) and euthanized by decapitation 5 wk after the initial STZ or

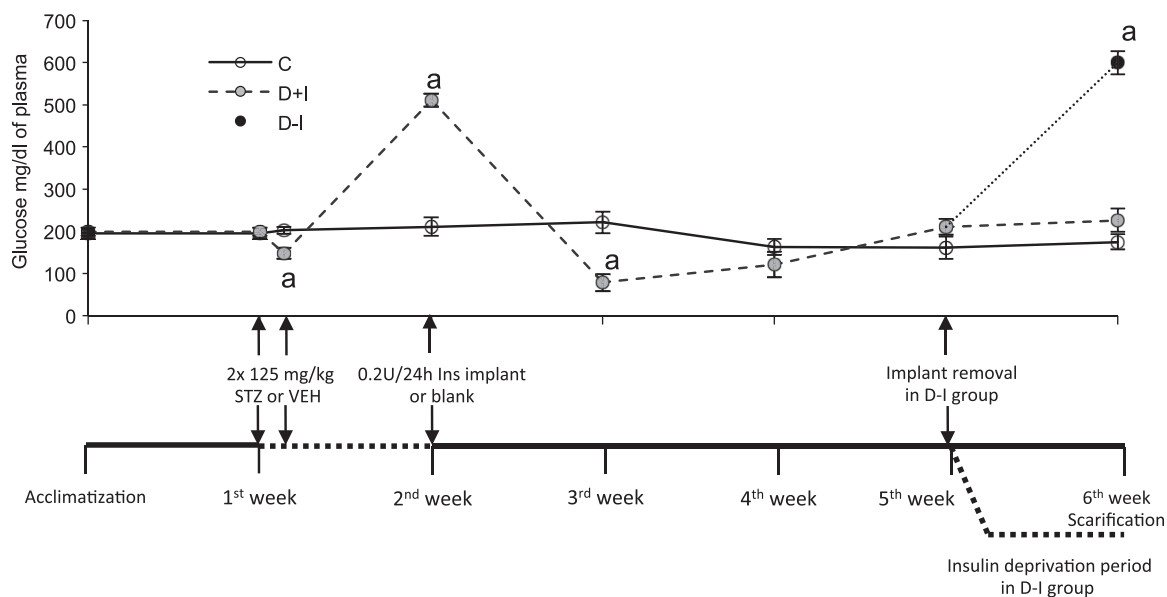


Fig. 1. Experimental design and time scale and exemplary blood glucose profile of control (C; $n = 3$) (solid line, \circ), insulin-treated (weeks 1–5: combined D + I and D - I groups under insulin treatment, $n = 6$; week 6: D + I group only, $n = 3$) (dashed line, gray circles), and insulin-deprived animals (D - I; $n = 3$) (dotted line, \bullet). STZ, intraperitoneal injection of streptozotocin; VEH, intraperitoneal injection of vehicle. Values represent means \pm SE. ^a $P < 0.05$ vs. C group by ANOVA.

vehicle dose. Figure 1 depicts the timeline of the experiment and blood glucose profiles for each experimental group. Additional animals were used for estimation of skeletal muscle insulin sensitivity by acute insulin stimulation. The mice were divided into the C ($n = 6$), D - I ($n = 7$), and D + I ($n = 7$) groups and followed appropriate experimental treatment, except for acute insulin stimulation 10 min prior to euthanization by pentobarbital overdose.

Isolation of muscle sarcoplasmic fraction and purification of mitochondria. Mitochondria were isolated from quadriceps muscle by differential centrifugation, as described previously (38). Briefly, quadriceps muscle samples were homogenized on ice using a motor-driven Potter-Elvehjem tissue grinder. After initial centrifugation, the supernatant containing the mitochondrial and sarcoplasmic fraction was transferred to a chilled microcentrifuge tube and centrifuged at 10,000 g for 2 min to pellet mitochondria. The supernatant containing sarcoplasmic fraction was frozen for further analysis. Mitochondrial pellet was washed twice by resuspending/centrifugation and finally suspended in a mitochondrial storage buffer. The levels of both the LCFa-CoA and sphingolipids in homogenates and various muscle fractions were normalized to total protein content, as measured by 660 nm Protein Assay (Thermo Scientific; Pierce Protein Biology Products, Rockford, IL).

Measurement of plasma FFA and tissue LCFa-CoA content by LC/MS/MS. Plasma free fatty acid concentrations were measured by liquid chromatography/mass spectrometry (LC/MS), as described previously (51). Briefly, 50 μ l of plasma was spiked with heptadecanoate internal standard (ISTD) and analyzed with Applied Biosystems (Foster City, CA) API5000 mass spectrometer coupled with a Cohesive (Franklin, MA) TX2 liquid chromatography system. Concentration of individual FFA was measured against a six-point standard curve prepared for each analyte. Both the ISTD and individual FFA standard curves were prepared in 2% fatty acid-free human albumin solution. All analytes were monitored as their $[M - H]^-$ ions.

LCFa-CoA esters were estimated using the LC-MS/MS method (9). After extraction in the presence of internal standard (20 ng of heptadecanoyl-CoA), samples were analyzed by UHPLC-ESI-MS/MS operating in multiple reaction monitoring mode [Waters Acquity UHPLC, C8 UPLC BEH column 2.1 \times 150 mm, 1.7 μ m (Waters, Milford, MA) and TSQ Quantum Ultra triple-quad mass spectrometer (Thermo Fisher Scientific, Waltham, MA)]. All standard curves were prepared using chemicals from Avanti Polar Lipids.

Measurement of sphingolipid content by LC-MS/MS. Quantity of sphingoid backbones [i.e., sphingosine (Sph) and sphinganine (dh-Sph)], together with individual molecular species of ceramide (Cer), was measured with the use of LC-MS/MS (10). Briefly, pure homogenates and sarcoplasmic and mitochondrial fraction aliquots were spiked with internal standards for sphingoid backbones and ceramides [dihydro 17C-sphingosine (d17:1-Sph) and margaric ceramide (C17:0-Cer)]. After extraction, samples were analyzed by UHPLC-ESI-MS/MS (Waters Acquity UHPLC, C8 UPLC BEH column 2.1 \times 150 mm, 1.7 μ m, Waters, and TSQ Quantum Ultra triple-quad mass spectrometer) working in MRM mode. All standard curves were prepared using standards obtained from Avanti Polar Lipids. All other chemicals were from Sigma-Aldrich (St. Louis, MO).

Immunoblotting. Frozen muscle tissue was pulverized in liquid nitrogen and sonicated on ice (Model 100 Sonic Dismembrator; Fisher Scientific) in RIPA buffer (Sigma-Aldrich) containing 5 mM TCEP (Thermo Fisher Scientific, Waltham, MA) and protease and phosphatase inhibitors (Complete Mini protease inhibitors cocktail tablets and PhosphoSTOP phosphatase inhibitor cocktail tablets; Roche Applied Science, Indianapolis, IN). After incubation at 4°C for 30 min, samples were centrifuged at 15000g to remove cell debris. Protein content in the resulting supernatant was measured using Pierce 660nm Protein Assay Kit (Thermo Fisher Scientific, Rockford, IL). Samples were prepared for SDS-PAGE in NuPAGE LDS Sample Buffer with 5 mM TCEP at a final protein concentration of 3 μ g/ μ l and denatured by heating at 70°C for 10 min. A total of 45 μ g of protein (15 μ l

total) was added to each well of precast gels (4–12% NuPAGE Novex Bis-Tris Midi Gels; Invitrogen, Carlsbad, CA). Proteins were separated by electrophoresis and blotted to nitrocellulose membranes. Membranes were blocked with 5% fat-free milk before incubating overnight with primary rabbit anti-mouse antibodies for proteins of intracellular fatty acid uptake (CD36, ab64014; Abcam, Cambridge, MA), acyl-CoA synthase (FATP1/ACSVL5, M-100; Santa Cruz Biotechnology, Dallas, TX), sphingolipid de novo synthesis [serine palmitoyltransferase (SPT) 10005260; Cayman Chemical, Ann Arbor, MI], ceramide synthesis (CerS1-NBP1-59733 and CerS5-NBP1-76964; Novus Biologicals, Littleton, CO), insulin sensitivity [Akt (Pan)] no. 2920, phospho-Akt (Ser⁴⁷³) no. 4060, GSK-3 α/β no. 5676, phospho-GSK-3 β (Ser⁹) no. 5558 (Cell Signaling Technology, Danvers, MA), and housekeeping protein (Vinculin, AB6039; Merck, Darmstadt, Germany). Proteins were detected using infrared fluorescent detection (Li-Cor Odyssey, Lincoln, NE) using appropriate anti-mouse and anti-rabbit secondary antibodies. Proteins were normalized to muscle vinculin expression (a focal adhesion plaque protein), which compared with GAPDH did not display variability between experimental groups (data not shown), and expressed as fold change over control group values.

Acute insulin stimulation. For acute insulin stimulation, the mice were fasted for 6 h and given human recombinant insulin (1 U/kg) by intraperitoneal injection, as described by Zong et al. (80). Ten minutes later the animals were euthanized by pentobarbital sodium overdose, and tissue samples were collected and subjected to immunoblotting and immunofluorescence analysis.

Gene transcript expression. Muscle tissue RNA was isolated using RNeasy Mini Kit (Qiagen, Hilden, Germany) according to the manufacturer's guidelines. Taqman Reverse transcription kit (Life Technologies, Carlsbad, CA) was used to prepare cDNA according to manufacturer's instructions. Real-time PCR was performed on the Viia7 Real Time PCR system (Life Technologies) using the Taqman Gene Expression Assays for glucose transporter type 4 (GLUT4; Mm01245502_m1), glycogen synthase 1 (GYS1; Mm01962575_s1), and insulin receptor substrate 1 (IRS-1; Mm01278327_m1). Values were normalized to β 2-microglobulin mRNA expression (Mm00437762_m1).

Principal component analysis. We employed multivariate modeling in form of principal component analysis (PCA) to estimate interdependence between variables and groups. Analysis was performed using Statistica 10.0 software package, using noniterative partial least squares algorithm. Noniterative partial least squares algorithm maximum number of iterations and convergence criterion were set at 50 and 0.0001, respectively. The number of principal components was determined using the Krzanowski cross-validation method. Results were presented as both the scores biplot to visualize relationships between individual animals and loadings plot to visualize relationships between variables. To prevent an artificial increase in the PCA model strength, we excluded a majority of closely interdependent variables.

Statistical analysis. Statistical significance between groups was estimated using ANOVA with the Tukey honestly significant difference post hoc test. We used Pearson's approach to establish relationships between selected variables chosen on the basis of PCA to estimate statistical relationship. Significance level was set to $P < 0.05$.

RESULTS

Anthropometric parameters. When compared with control animals, insulin-deprived diabetic mice displayed significantly lower total body weight, fat and lean tissue mass, and total body water ($P < 0.001$ in all cases; Table 1). The drop in total body water as seen in D - I group and increase in bladder water volume had no impact on body hydration ratio, which was not different from the C group. When values were ex-

Table 1. Anthropometric parameters of C, D – I, and D + I animals on the day of euthanization

	C	D – I	D + I
Body weight, g	25.1 ± 0.5	20.7 ± 0.7^{a,b}	23.0 ± 0.4^a
Fat, g	2.7 ± 0.2	0.9 ± 0.1^{a,b}	2.3 ± 0.1
Lean, g	20.1 ± 0.2	16.6 ± 0.6^{a,b}	19.2 ± 0.1
Body water, g	17.1 ± 0.5	14.3 ± 0.5^a	15.7 ± 0.3
Bladder water, g	0.07 ± 0.03	0.17 ± 0.06^a	0.15 ± 0.05
Fat (%)	10.6 ± 0.8	4.3 ± 0.3^{a,b}	9.7 ± 0.5
Lean (%)	80.1 ± 0.9	82.6 ± 0.6	82.2 ± 0.7
Water (%)	68.1 ± 1.8	71.1 ± 1.8	67.4 ± 1.3
Hydration ratio (%)	84.2 ± 2.2	83.8 ± 1.9	80.8 ± 1.1
Glucose, mg/dl	160 ± 11	706 ± 13^{a,b}	150 ± 20
Ketones, mmol/l	0.2 ± 0.0	0.5 ± 0.1^{a,b}	0.2 ± 0.0
Hb A _{1c} , (%Hb)	4.6 ± 0.0	7.7 ± 0.3^{a,b}	5.7 ± 0.2^a
Food intake, g/24 h	3.56 ± 0.21	6.68 ± 0.54^{a,b}	3.78 ± 0.22

Values are means ± SE ($n = 8$ /group). C, control; D – I, streptozotocin type 1 diabetic insulin-deprived animals; D + I, streptozotocin type 1 diabetic insulin-treated animals. Significant values are in boldface. ^a $P < 0.05$ vs. C group; ^b $P < 0.05$ vs. D + I group. Food intake was calculated as mean from the last 3 days of the experiment.

pressed in percentage of total body mass, only the decrease in fat content and increase in bladder water volume were significantly different between the D – I and C groups. Insulin deprivation significantly elevated plasma glucose, ketones and %Hb A_{1c} values compared with the C group ($P < 0.001$ in all cases). Insulin treatment normalized all body composition and blood parameters in D + I animals except total body mass and Hb A_{1c} value.

Impact of STZ diabetes on plasma fatty acid composition. Compared with control, total content of plasma FFA doubled under the insulin deprivation state ($P < 0.01$; Fig. 2A). The most prominent increase was noted for all 18-carbon chain FFAs ($P < 0.01$ in each case) and was responsible for ~80% of the total FFA concentration change. Percentage composition of plasma FFAs was also affected, with all non-18-carbon FFA displaying significant decreases in their percentage yield ($P < 0.01$ in each case), with linoleate (C18:2) and linolenate (C18:3) showing significant increase ($P < 0.001$ in both cases; Table 2). Those changes increased FFA UI by 15% ($P < 0.001$). Insulin treatment completely reversed the changes in plasma FFA concentration introduced by insulin deprivation (Fig. 2A). Despite insulin treatment, the percentage yield of C14, C16, and C16:1 FFA in D + I group was still significantly lower ($P < 0.01$), whereas the percentage yield of C18:2 FFA was significantly higher ($P < 0.001$). FFA UI was still significantly higher in D + I group compared with control (by 7%, $P < 0.05$; Table 2).

Insulin deprivation increases the content and UI of LCFa-CoAs in skeletal muscle. Insulin deprivation more than doubled the total content of LCFa-CoA esters in mouse quadriceps compared with control animals ($P < 0.001$; Fig. 2B, black bars). Differences were most prominent for C16:1-CoA, C18:1-CoA, C18-CoA, and C18:2-CoA esters ($P < 0.001$ in all cases). Percentage of monounsaturated palmitoleoyl and oleoyl ester was significantly higher (by ~10%, $P < 0.001$ in both cases), whereas percentage of saturated palmitoyl and arachidonoyl esters was significantly lower (by 27% $P < 0.001$ in both cases; Table 2), compared with the control values. Overall LCFa-CoA UI increased by 4% ($P < 0.001$; Table 2). Insulin treatment normalized the content of almost all LCFa-CoAs.

Only oleoyl, stearoyl, and linoleoyl LCFa-CoA esters were still higher than the control values ($P < 0.001$ in all cases). Those 18-carbon molecular species of LCFa-CoAs were responsible for the increase in both the total content of LCFa-CoA (by 52%, $P < 0.001$) and UI (by 4%, $P < 0.001$) in the D + I group compared with the C values.

Ceramide content in both total homogenate and muscle sarcoplasmic fraction increases during insulin deprivation and is normalized by insulin treatment. One week of insulin withdrawal in T1D increased the total content of ceramide in quadriceps muscle significantly ($P < 0.001$; Fig. 3A). The most affected molecular species were C18:0, C18:1, and C24:0-ceramide ($P < 0.001$ in all cases). Insulin deprivation elevated the content of saturated fatty acid ceramides more than those with unsaturated ones, leading to the decrease of UI compared with the control group (by 17%, $P < 0.05$; Table 2). Insulin treatment decreased the total ceramide content to the levels observed in the control group (Fig. 3A). Ceramide UI was still lower (by 14%, $P < 0.05$). Interestingly, dhSph, an intermediate in de novo synthesis of ceramide, was increased significantly in the muscle of insulin-treated animals (by 27% vs. C group, $P < 0.05$; Fig. 3B).

The impact of insulin deprivation on the content of sphingolipids was most visible in the sarcoplasmic fraction, the site of de novo sphingolipid synthesis catalyzed by combined action of SPT and ceramide synthases (CerS). Insulin depriva-

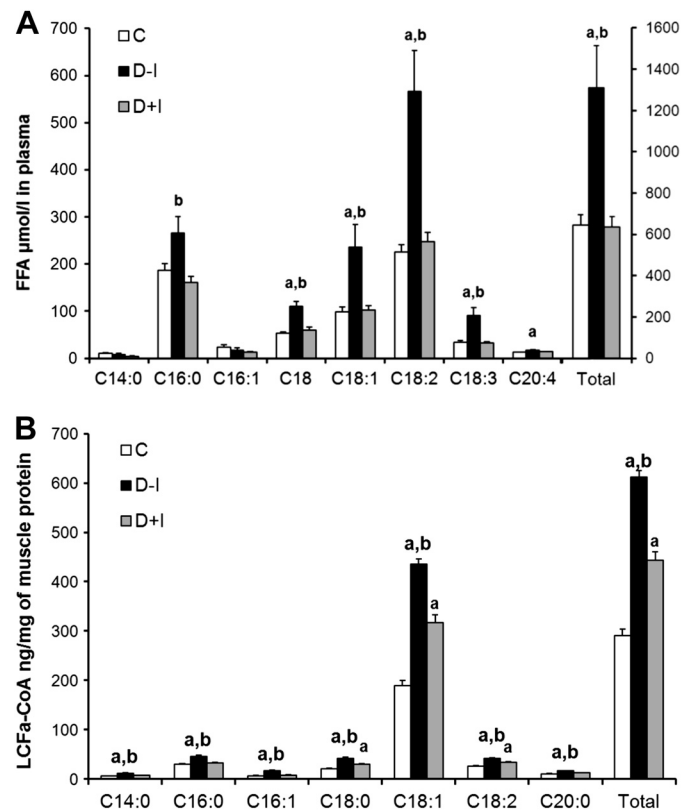


Fig. 2. Insulin deprivation affects both the content and composition of plasma free fatty acids (FFA; A) and skeletal muscle long-chain fatty acids-acyl-CoA esters (LCFa-CoA; B) in diabetic C57Bl/6J mice. Values are expressed in $\mu\text{mol/l}$ of plasma for FFA (means ± SE; $n = 8$ /group) or ng/mg of protein for LCFa-CoA (means ± SE; $n = 13$ /group). ^a $P < 0.05$ vs. C group; ^b $P < 0.05$ vs. D + I group.

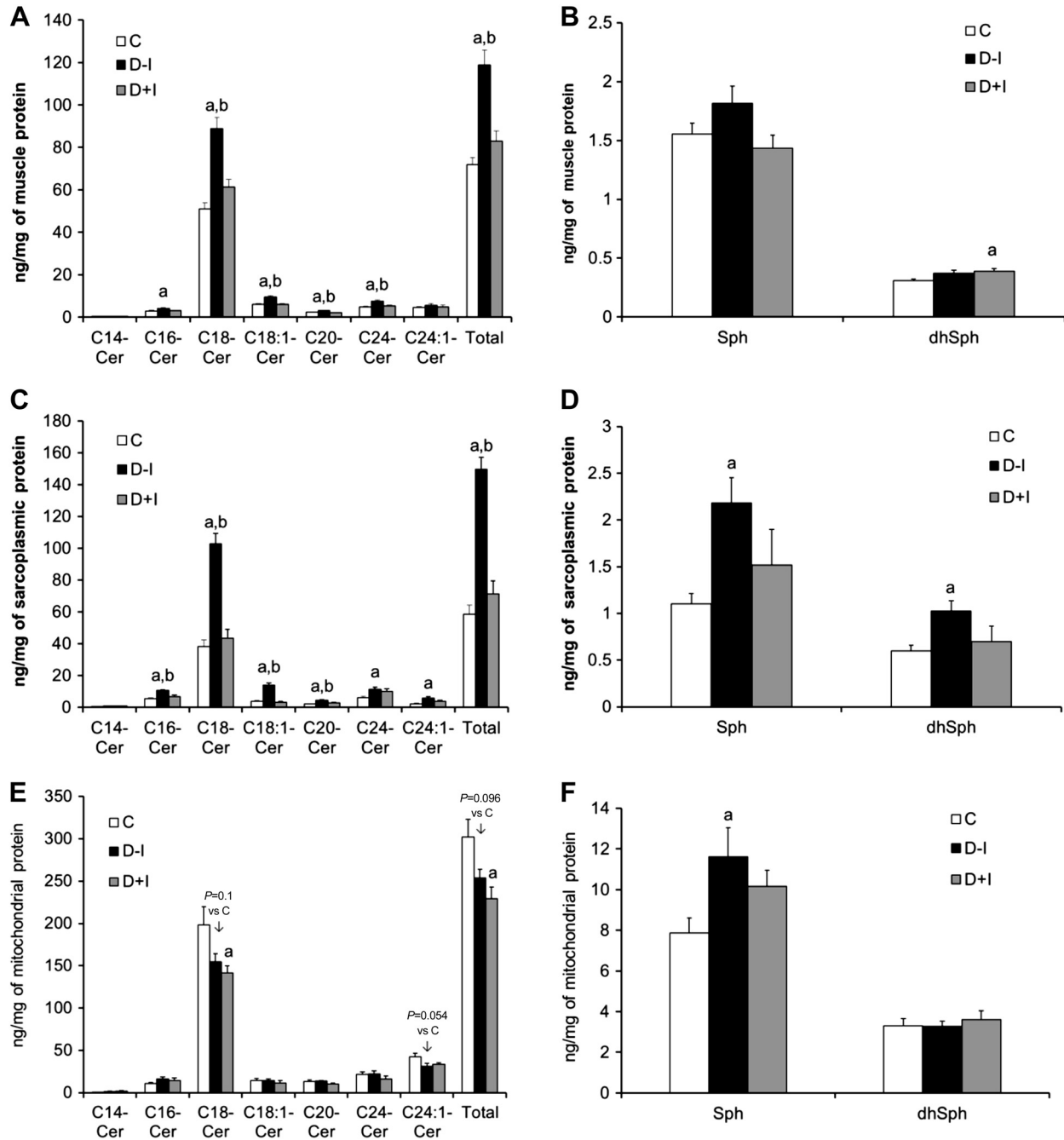


Fig. 3. Insulin deprivation increases the content of ceramide in mouse skeletal muscle homogenates and sarcoplasmic fraction but not in mitochondria. Shown is the impact of insulin deprivation (black bars) and insulin treatment (gray bars) on the content of individual ceramide (Cer) molecular species (left) and sphingoid bases (right) in mouse quadriceps muscle homogenates (A and B), sarcoplasmic fraction (C and D), and mitochondrial fraction (E and F). Values were normalized to protein content in appropriate fraction and represent the mean ng/mg of protein content \pm SE; $n = 13/\text{group}$; ^a $P < 0.05$ vs. C group; ^b $P < 0.05$ vs. D + I group.

animals, whereas GLUT4 mRNA level increased only moderately (Fig. 4C).

Insulin signaling in STZ-diabetic animals is inhibited in both insulin-deprived and insulin-treated states. To evaluate how the alternations at the muscular lipid level influence skeletal muscle insulin sensitivity, we performed acute insulin stimulation in an additional group of animals. Both diabetic-deprived and diabetic-treated animals displayed decreased phosphorylation of protein kinase B (p-Akt/Akt, by $\sim 40\%$, $P < 0.05$;

Fig. 4D) and glycogen synthase kinase-3 β (p-GSK-3 β /GSK-3 β , by $\sim 20\%$, $P < 0.05$). This indicates lower insulin sensitivity or insulin resistance in both experimental groups.

PCA and correlation analysis reveal close relationship between sarcoplasmic ceramide levels, expression of ceramide synthesis enzymes, and diabetic phenotype parameters. Three major principal components identified were responsible for a total of 59.3% of cumulative variance within the data set (pc1 = 39.1%, pc2 = 10.4%, pc3 = 9.67%; cumulative R2X = 0.593,

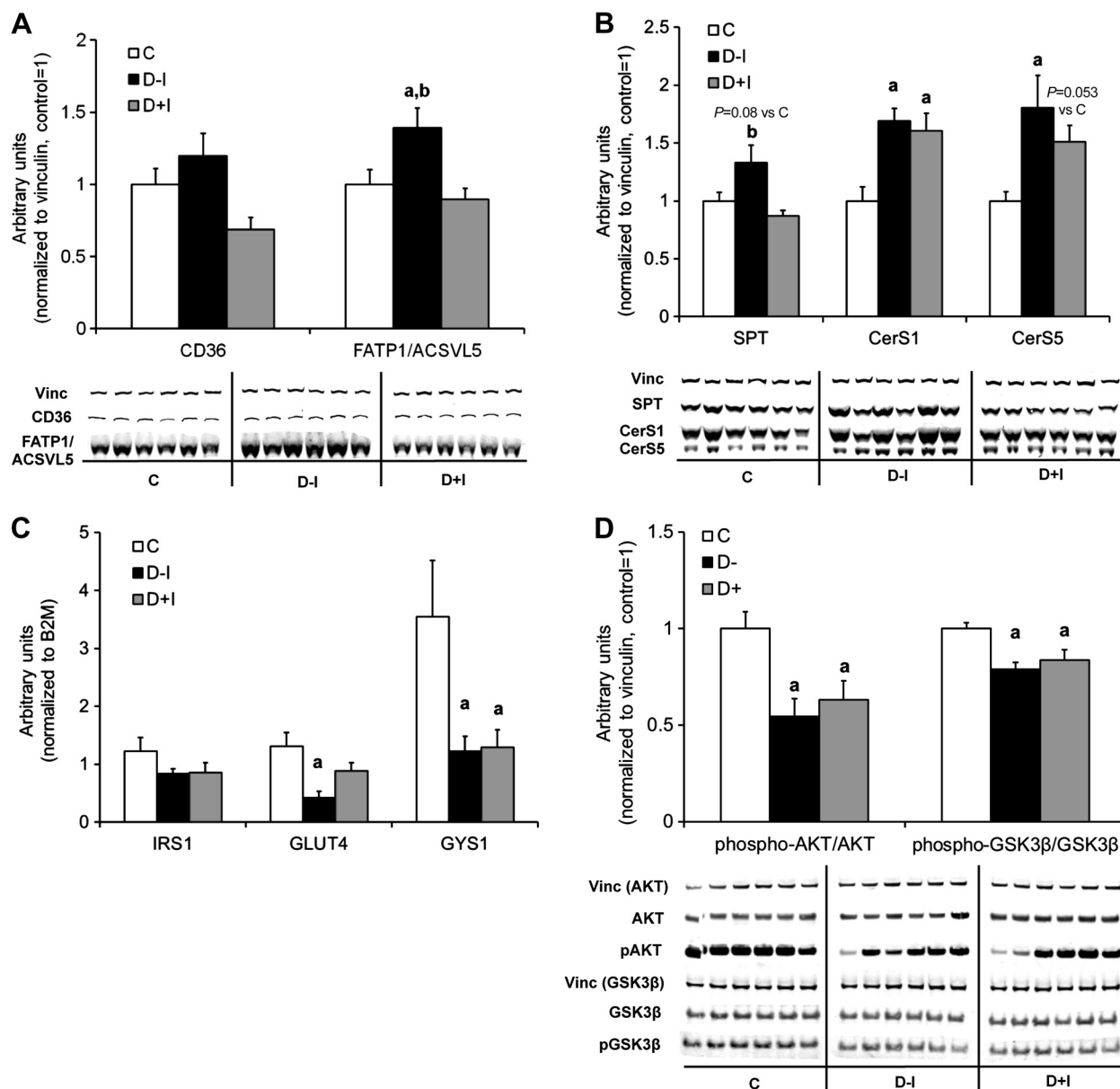


Fig. 4. Insulin deprivation upregulates proteins of LCFa-CoA and Cer synthesis and affects the genes and proteins implicated in muscle insulin sensitivity. The impact of insulin deprivation and treatment on content of proteins of intramyocellular FFA uptake and LCFa-CoA synthesis (CD36 and FATP1/ACSVL5; A), sphingoid backbone formation and Cer synthesis [serine palmitoyltransferase (SPT), CerS1, and CerS5; B], genes implicated in muscle tissue insulin sensitivity [insulin receptor substrate-1 (IRS-1), glucose transporter type 4 (GLUT4), and glycogen synthase 1 (GYS1); C], and Akt-dependent insulin signaling (phosphorylation state of Akt and its downstream target GSK-3 β ; D) in mouse skeletal muscle. Values were normalized to vinculin expression for protein data and β 2-microglobulin for mRNA data. Bars represent SE; $n = 8$ /group (except for D; see MATERIALS AND METHODS). ^a $P < 0.05$ vs. C group; ^b $P < 0.05$ vs. D + I group.

Q2 = 0.319). Score biplot shows wide separation between D – I and D + I animals (Fig. 5). Diabetic-treated animals clustered near control ones, yet they did not create a single cluster, suggesting that despite similar behavior of variables in the D + I and C groups, insulin treatment did not fully rescue the phenotype. Overlay of variable vectors shows that factors that mostly differentiate the D – I group from D + I and C groups (along the t1 axis; Fig. 5) were diabetes-related variables such as %Hb A_{1c}, plasma FFA, body fat content, and muscular lipid-related variables such as the content of LCFa-CoA and sarcoplasmic ceramide (both total and C18-FA-containing species), the content of lipid synthesis enzymes (SPT, FATP1/

ACSVL5, CerS), and mRNA expression of proteins implicated in muscle insulin resistance. Mitochondrial sphingolipids (total and individual molecular species) and CD36 protein expression had the least impact on between-group differentiation but were the major factors describing within-group differentiation (along the t2 axis; Fig. 5).

Loadings scatter plot revealed clustering of D – I group with features characteristic for diabetic phenotype (plasma glucose, %Hb A_{1c}) together with sarcoplasmic ceramide and homogenate LCFa-CoA content (both the total and 18-carbon molecular species content). Those variables were the members of feature cluster 1 (Fig. 6), which also included other molec-

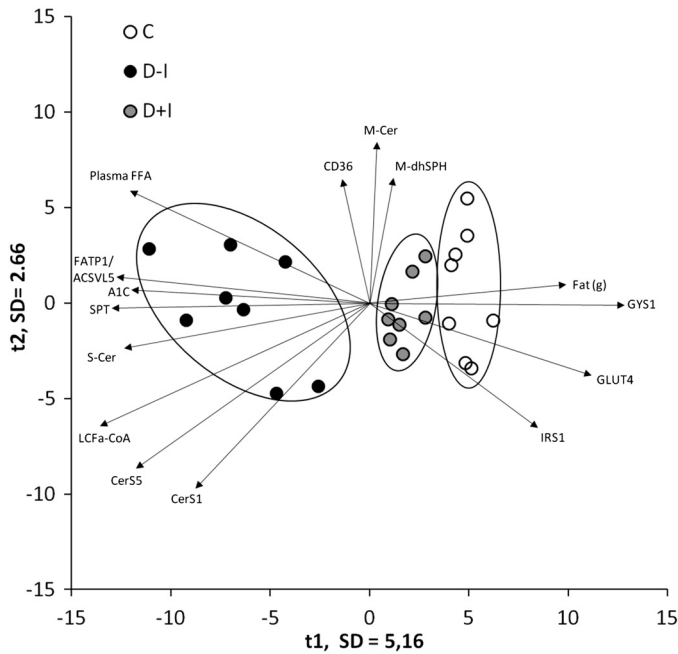


Fig. 5. Scores scatter plot for 1st and 2nd components of principal component analysis: ●, individual D – I animals; gray circles, individual D + I animals; ○, individual C animals. Ovals represent clustering of animals from respective experimental groups. Arrows indicate directions of major variables that are responsible for between- and within-group differences. S-Cer, total sarcoplasmic ceramide; M-Cer, total mitochondrial ceramide; M-dhSPH, mitochondrial sphinganine.

ular species of sarcoplasmic Cer and LCFA-CoA and the proteins involved in their synthesis. Other notable clusters were plasma ketones and the FFA cluster (cluster no. 2; Fig. 6), which contained total content and a majority of molecular species of FFA together with 18:1-Cer in sarcoplasmic fraction. All the above-mentioned features were in apposition to each other and opposite to both the D + I and C group representations (along the first-principle component axis). Both the C and D + I groups were the members of features cluster no. 3 (Fig. 6A), which included variable characteristics of nondiabetic phenotypes such as high mRNA expression of genes implicated in muscle insulin sensitivity (IRS-1, GLUT4, GYS1), major body composition parameters (fat, lean tissue, and total body weight) and %SAT in plasma FFA and tissue LCFA-CoA. This suggests negative correlation of the above-mentioned variables with diabetic phenotype and positive correlation with control or diabetic-treated groups. Except for the plasma FFA UI, this parameter in LCFA-CoA and Cer in all fractions did not cluster with features of the diabetic phenotype. The same was observed for mitochondrial sphingolipid parameters and CD36 protein content.

Results of PCA suggest a close relationship between the plasma content of FFA, muscular content of LCFA-CoA, and ceramides in both the total homogenate and sarcoplasmic fractions. We used Pearson approach to further confirm interdependence of those variables. LCFA-CoA in homogenates showed a strong, positive correlation with total ceramide content in both the homogenates ($r = 0.780, P < 0.001$; Fig. 7B) and sarcoplasmic fraction ($r = 0.726, P < 0.001$; Fig. 7C) and weaker yet still significant positive correlation with total plasma FFA ($r = 0.560, P < 0.05$; Fig. 7A). At the level of

proteins, FATP1/ACSVL5 and SPT protein content were highly correlated with each other ($r = 0.867, P < 0.001$) and with both total and 18-carbon molecular species of plasma FFA (mean $r \approx 0.7$, both the FATP1/ACSVL5 and SPT, $P < 0.001$ in both cases). SPT, CerS1, and CerS5 protein expression displayed significant, positive correlation with sarcoplasmic ceramide content (mean $r \approx 0.6, P < 0.01$).

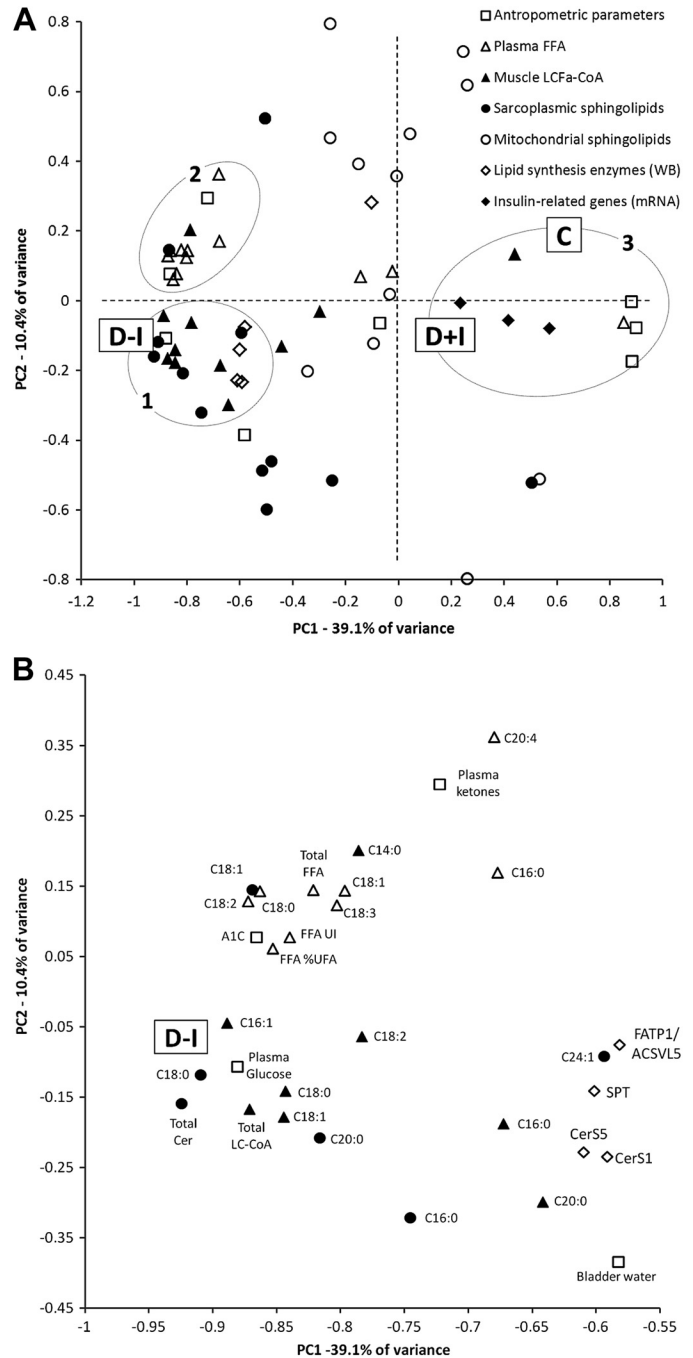


Fig. 6. Loadings scatterplot for first 2 components show clustering of the diabetic phenotype, muscle lipid-related variables, and representation of a diabetic group (D – I). A: scatterplot of all variables. The variables grouped in 3 major clusters (encircled) are described in RESULTS. B: for better visibility, the variables from clusters 1 and 2 are displayed. PC1, principal component 1 axis; PC2, principal component 2 axis.

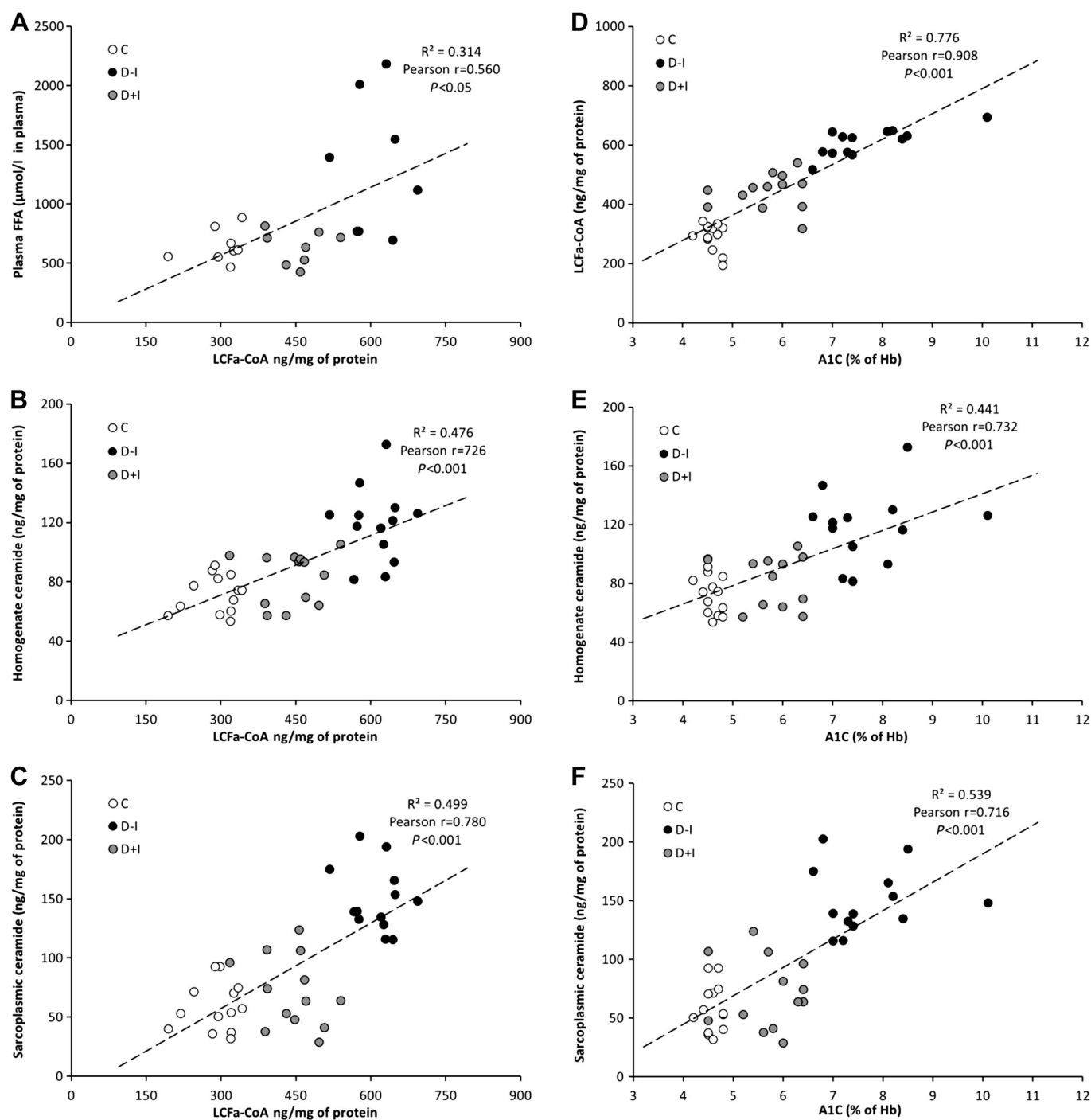


Fig. 7. Muscle content of LCFa-CoA is highly correlated with both muscle sarcoplasmic ceramide content and blood %Hb A_{1c} value. *Left*: correlations between muscle total content of LCFa-CoA and total plasma FFA (A), total muscle ceramide (B), and muscle total sarcoplasmic ceramide (C). *Right*: relationship between blood %Hb A_{1c} and the total content of muscle LCFa-CoA (D), muscle ceramide (E), and sarcoplasmic ceramide (F). Linear regression scores (r^2), Pearson r values, and their respective P values are shown next to the linear regression plots. \circ , Nondiabetic C animals; gray circles, D + I animals; \bullet , D - I animals.

Because daily plasma glucose values depend on food intake, we used %Hb A_{1c} level in establishing a relationship between glycemic control and lipid parameters. %Hb A_{1c} displayed the strongest positive correlation with total muscle content of LCFa-CoA, total muscle ceramide, and sarcoplasmic ceramide, with Pearson's correlation $r = 0.908$, $r = 0.732$, and $r = 0.716$ respectively ($P < 0.001$ in all cases; Fig. 7, D, E, and F, respectively). Notably, all of the 18-carbon molecular species

of FFA, LCFa-CoA, and ceramides had the strongest correlation with %Hb A_{1c} values, ranging from $r = 0.890$ for C18:1 LCFa-CoA to $r = 0.690$ for sarcoplasmic C18:0-Cer (mean: $r = 0.736$, $P < 0.001$ in all cases), which was not pronounced for palmitate-containing lipids (mean $r = 0.589$, $P < 0.05$ for palmitoyl-CoA and sarcoplasmic palmitoyl-ceramide only). Although plasma FFAs were only weakly, positively correlated with %Hb A_{1c} values ($r = 0.593$, $P < 0.05$), both total and

percentage body fat had strong, negative correlations ($r = -0.773$ and $r = -0.754$, respectively, $P < 0.001$ in both cases), and ketones had a strong positive correlation ($r = 0.812$, $P < 0.001$) with glycosylated hemoglobin level. It has to be noted that although the above-mentioned variables displayed high reciprocal correlation, the effect was visible only when all three groups were introduced into correlation analysis but were absent when only the values from single group were taken into consideration. Lipids containing stearate or oleate moieties displayed strong reciprocal interdependence between different extra- and intracellular pools and across measured compounds ranging from $r = 0.826$ for plasma stearate and sarcoplasmic stearyl-ceramide to $r = 0.524$ for plasma oleate and tissue oleoyl-CoA (mean: $r = 0.782$ for stearate-containing lipids and $r = 0.694$ for oleate-containing lipids). This was not observed for lipids with palmitate moiety.

DISCUSSION

The major findings of the current study are that 1) insulin deprivation elevates plasma FFA, which correlates with the increase in the muscle LCFa-CoA and ceramide content in both the total homogenates and sarcoplasmic fraction; 2) the changes were accompanied by an increase in the protein expression of lipid-synthesizing enzymes and a decrease in the expression of genes implicated in muscle insulin sensitivity; 3) lipid species based on stearic and oleic fatty acids display the greatest degree of change both in content and in percentage; 4) insulin treatment normalizes both plasma FFA and sphingolipid alternations in muscle but has lesser influence on muscular LCFa-CoA content and composition, protein expression of CerS, gene expression of GYS1, and Akt-dependent insulin signaling; 5) insulin deprivation and treatment has substantial impact on sphingolipid content and composition in sarcoplasmic fraction, but less so in the mitochondrial fraction; and 6) principal component and correlation analysis reveals a close relationship between features of diabetic phenotype such as %Hb A_{1c} and both the muscle LCFa-CoA and ceramide content in the sarcoplasmic fraction but not in the mitochondrial one. Altogether, these results offer a mechanistic link between sphingolipids, LCFa-CoAs, and the diabetic phenotype, which is a potential explanation for the predisposition to insulin resistance in type 1 diabetes.

The substantial decline in fat mass observed in the current study during insulin deprivation could be explained by both the lack of insulin action on adipose tissue hormone-sensitive lipase and fatty acid esterification (32). The insulin-deprived animals displayed specific increases in all 18-carbon plasma FFAs, which can be explained by dietary fat composition. Oleate and linoleate fatty acids account for 80% molar content of soybean oil used in TD.10112 chow, with palmitate, stearate, and linolenate accounting for the remaining 20%. It has been reported that increased intracellular drive of FFAs during the insulin-deprived state is connected not only with passive, diffusion-based flip-flop mechanism but also with increased expression and membrane translocation of fatty acid transporters CD36 and FABPpm, as seen in T1D individuals (25, 44). Although in the current study we did not observe alternations in CD36 expression, the protein content of acyl-CoA synthase FATP1/ACSVL5 was significantly elevated during insulin deprivation. Intracellular FFAs are transformed to acyl-CoA

esters by acyl-CoA synthetase activity, and our results demonstrate a close relationship between plasma FFAs and muscular LCFa-CoA level, a feature most prominent for their 18-carbon species. An increase in the content of LCFa-CoA was observed previously in rat heart from STZ T1D animals (47), in skeletal muscle of insulin-resistant diabetic Zucker rats (5), and in soleus muscle preincubated with oleate and linoleate (69). Accumulation of muscular LCFa-CoA can contribute to muscle insulin resistance, as shown by Ellis et al. (21), where high-fat diet-induced insulin resistance was accompanied by the increase in activity of acyl-CoA synthase and elevation in rat gastrocnemius muscle LCFa-CoA. Similar to the current study, the most affected molecular species of acyl-CoAs were 18-carbon unsaturated CoAs (e.g., 18:1-CoA and 18:2-CoA). Acyl-CoAs diminish the effect of insulin on muscle glucose uptake by inhibiting hexokinase activity (68) and by activation of various PKC isoforms, which interferes with insulin signaling (57). Activation of PKC ϵ and PKC θ concomitant with the elevation of muscular LCFa-CoAs was observed by Laybutt et al. (39) in skeletal muscle of rats made insulin resistant by chronic glucose infusion or high-fat diet (58). Other groups reported that 4 h of lipid infusion in rats leads to accumulation of 18:2-CoA, PKC θ membrane translocation, inhibition of insulin-signaling cascade at IRS-1 level, and a decrease in muscle glucose uptake (42, 77), whereas PKC θ knockout mice are resistant to fat-induced insulin resistance (35). In vitro studies confirmed that both the palmitoyl-CoA and oleoyl-CoA can directly activate various PKC isoforms with similar potency as classic PKC activators, Ca²⁺, diacylglycerol, and phosphatidylcholine (74). The current study demonstrated for the first time, to the best of our knowledge, that the insulin deprivation-related increase in plasma FFA is accompanied by LCFa-CoA accumulation in skeletal muscle, which is most visible for oleoyl-CoA. Interestingly, the current study has also shown that insulin deprivation-related alternations in muscular LCFa-CoA content and composition are not completely reversed by insulin treatment, which suggests that a similar mechanism could potentially occur in long-term insulin-treated T1D subjects and can contribute to muscle insulin resistance.

Ceramides are also recognized as potent inducers of muscle insulin resistance. Ceramides are released as products of complex sphingolipid hydrolysis or synthesized from sphingoid base (Sph or dhSph) and LCFa-CoA at the level of sarcoplasmic reticulum (45). The rise in circulating FFA and elevated muscle ceramide levels was observed previously in soleus and red gastrocnemius skeletal muscle of streptozotocin-diabetic rats (8, 16) and in muscle-specific insulin receptor knockout mice and streptozotocin-treated mice (23). De novo sphingolipid synthesis depends on the supply of LCFa-CoA for both the sphingosine backbone formation by SPT and subsequent sphingosine acylation to yield ceramide. The latter is catalyzed by various isoforms of sarcoplasmic CerS. CerS1 and CerS5 account for ~50 and 25% of total ceramide synthase activity, respectively, in skeletal muscle and in vitro synthesize ceramides with C14 to C20 acyl chain length (49). CerS1 and -5 display the highest substrate specificity toward Sph, C18-CoAs, and C16-CoAs. Upregulation of both CerS isoforms by insulin deprivation resulted in the acute increase in C16, C18, and C18:1 ceramides in mouse quadriceps, which was most prominent in the muscle sarcoplasmic fraction, the place of

ceramide synthesis. The strong, positive interdependence between muscle SPT, the content of ceramide, and insulin resistance was reported previously by Holland et al. (29) in various models of insulin resistance in mice. The current study shows for the first time that muscular ceramide content is highly correlated with the plasma FFA, muscular LCFa-CoAs, and muscle SPT and CerS protein expression in streptozotocin-diabetic mice when all three experimental groups are included in correlation analysis. Ceramide accumulation in muscle can be reversed by insulin treatment. This relationship is more prominent for sarcoplasmic than total muscle ceramide and is not observed in mitochondria. Mitochondria contain several sphingolipid-metabolizing enzymes and are not directly connected with sarcoplasmic sphingolipid pool by Golgi membrane vesicular transport (7, 26). The current data suggest distinct regulation of mitochondrial sphingolipid metabolism in muscle from that of sarcoplasm, where sphingolipid content and composition followed the alternations in LCFa-CoA level. Alternation of lipid synthesis is one of the events observed in ER stress response (22). Lipid-induced ER stress is known to be involved in both liver (43) and muscle (56, 78) insulin resistance. Ceramide accumulation with triggering of ER stress markers and inhibition of insulin signaling was observed in liver tissue biopsies from alcohol-related liver disease (ALD) patients (43) and in a rat model of ALD (54). Significant accumulation of sarcoplasmic ceramide observed in our study can promote muscle insulin resistance through ER stress response, yet elucidation of this mechanism requires further investigation.

Another intriguing observation is the finding that mutual interdependence of plasma FFA, muscular LCFa-CoA, and sarcoplasmic ceramides was most prominent for their 18-carbon molecular species, rather than for 16-carbon ones, as shown by correlation analysis. Until now, most studies have focused on palmitate and its involvement in intramuscular ceramide accumulation and induction of insulin resistance (1, 19, 53, 64), the rationale being that it can form both the sphingoid backbone (dhSph, through condensation of palmitoyl-CoA and L-serine by sarcoplasmic SPT) and palmitoyl-ceramide (through the activity of sarcoplasmic ceramide synthase), thus increasing ceramide content by two parallel mechanisms. Palmitate, but not oleate, was shown to increase ceramide accumulation in muscle myotubes (11), decrease phosphorylation of Akt (55), and induce muscle insulin resistance (52), the latter even improving palmitate-induced insulin resistance (6, 14, 55). On the contrary, a study by Thompson et al. (69) reported that oleate and linoleate were more potent inhibitors of insulin-stimulated glucose uptake, glucose phosphorylation, and glycogen synthesis in isolated soleus muscle than palmitate. Oleate and linoleate were also reported by Schmitz-Peiffer et al. (59) to inhibit both basal and insulin-stimulated glycogen synthesis, glucose uptake, and glucose phosphorylation. In the saturated form, 18-carbon stearate was shown to be as potent as palmitate in stimulation of ceramide synthesis. (11). In the current study, plasma stearate and oleate had greater degrees of correlation than palmitate, with the respective molecular species of LCFa-CoA and ceramide in both the total homogenates and sarcoplasmic fraction. Our results suggest that 18-carbon saturated and unsaturated fatty acids are more important in T1D-induced LCFa-CoA and muscle sphingolipid accumulation and display stronger correlation with diabetic phenotype descrip-

tors such as %Hb A_{1c}. This relationship is further reinforced by the results of PCA analysis, where lipid species containing stearic, oleic, or linoleic fatty acid moiety were among the top 10 variables that were most influential on PCA analysis outcome (data not shown).

We have reported in the current study the mRNA expression of proteins that are involved in insulin signaling. Because of the continuous release of insulin in implanted animals and long insulin washout time after implant removal (due to minute debris of implant material still present under the skin), the employment of the hyperinsulinemic euglycemic clamp was not feasible in our experimental model. A decrease in the gene and/or protein expression of IRS-1 with concomitant insulin resistance was observed in muscle biopsies of insulin-resistant Pima Indians (36), muscle of T2D subjects (33), and muscle biopsies from women with gestational diabetes (15). Similar concordance of mRNA gene expression of GLUT4 in the skeletal muscle of rats (41) and humans (15, 33) and for GYS mRNA expression in the muscle of T2D subjects (72) and insulin resistance has been reported. The decline observed in GLUT4 and GYS1 gene expression in the diabetic animals during insulin deprivation (D - I) indicates decreased muscle insulin sensitivity, which was confirmed by the status of Akt-related signaling under acute insulin stimulation. Insulin treatment of the diabetic mice (D + I) failed to normalize these declines in signaling protein mRNA expression or improve Akt signaling, which supports the finding that these animals remained insulin resistant despite peripheral insulin administration. The current study supports the notion that insulin resistance may contribute to the complication of type 1 diabetes even after replacing insulin.

The measure of glycosylated hemoglobin level (%Hb A_{1c}) is regarded as a gold standard to assess glycemic control in type 1 and type 2 diabetes (60). An increase in %Hb A_{1c} correlates with the prevalence of diabetic complications. Therefore, long-term normalization of %Hb A_{1c} level is a key goal in T1D treatment. Our data show that %Hb A_{1c} value is tightly correlated with muscle content of both the LCFa-CoA and ceramides in both total homogenates and sarcoplasmic fraction. Both the PCA results and correlation analysis also confirm the importance of stearate- and oleate-containing lipids, as those molecular species displayed the greatest correlation with the %Hb A_{1c} value and were major sphingolipids clustered with features of the diabetic phenotype. Finally, we were able to demonstrate that most of the lipid alternations introduced by insulin deprivation could be reversed by long-term insulin treatment. Animals from the D + I group did not differ from controls in total and percent fat content, plasma FFA, total homogenate, or sarcoplasmic ceramide levels. These data suggest that insulin inhibition of hormone-sensitive lipase and stimulation of fat tissue triglyceride synthesis channeled an excess of FFA toward storage and prevented intramyocellular sphingolipid accumulation. Of interest is that the muscle content of LCFa-CoA, although suppressed by insulin treatment, was still significantly higher in the D + I group. The insulin had no influence on percentage distribution or unsaturation index of LCFa-CoAs and only partially affected unsaturation of plasma FFA. These results suggest that many of the factors not corrected by insulin treatment may play important roles in developing insulin resistance in T1D individuals even when tight glycemic control is maintained. However, it is important

to recognize that STZ-diabetic mice are not true T1D individuals and that the pathophysiology of the two are different, although both result in insulin deficiency.

In summary, we demonstrate that insulin deprivation significantly affects both the content and percentage composition of skeletal muscle ceramide through an increase in the protein expression of enzymes involved in sphingolipid synthesis and is connected with reduced gene expression of proteins involved in muscle insulin sensitivity and Akt-related insulin signaling. PCA and correlation analysis revealed that alternations were connected with plasma FFA and muscular LCFa-CoA increase and were most visible for 18-carbon containing sphingolipids in sarcoplasmic fraction of the muscle. Although insulin treatment normalized many of the observed derangements in sphingolipids in diabetic mice, there were persistent changes in LCFa-CoA levels, ceramide synthesis enzymes, and insulin signaling proteins following insulin treatment that provide a potential explanation for the insulin resistance that manifests even after exogenous insulin treatment in type 1 diabetic individuals.

GRANTS

This work was supported by National Institute of Diabetes and Digestive and Kidney Diseases Grant R01-DK-41973, Center for Translational Science Activities Grant UL1 TR000135, the David Murdock Dole Professorship (K. S. Nair), and the Stephenson Fellowship (P. Zabielski).

DISCLOSURES

No conflicts of interest, financial or otherwise, are declared by the authors.

AUTHOR CONTRIBUTIONS

P.Z., I.R.L., K.A.K., and K.S.N. contributed to the conception and design of the research; P.Z., I.R.L., D.R.J., X.-M.P., J.G., K.A.K., and J.M.C.-S. performed the experiments; P.Z., A.U.B.-Z., I.R.L., S.G., S.M., D.R.J., X.-M.P., J.G., K.A.K., J.M.C.-S., M.D.J., and K.S.N. analyzed the data; P.Z., A.U.B.-Z., I.R.L., S.G., S.M., D.R.J., X.-M.P., J.G., K.A.K., M.D.J., and K.S.N. interpreted the results of the experiments; P.Z., I.R.L., K.A.K., and K.S.N. prepared the figures; P.Z., A.U.B.-Z., and K.S.N. drafted the manuscript; P.Z., A.U.B.-Z., I.R.L., S.G., S.M., D.R.J., X.-M.P., K.A.K., J.M.C.-S., M.D.J., and K.S.N. edited and revised the manuscript; P.Z., A.U.B.-Z., I.R.L., S.G., S.M., D.R.J., X.-M.P., J.G., K.A.K., M.D.J., and K.S.N. approved the final version of the manuscript.

REFERENCES

- Alkhateeb H, Chabowski A, Glatz JF, Luiken JF, Bonen A. Two phases of palmitate-induced insulin resistance in skeletal muscle: impaired GLUT4 translocation is followed by a reduced GLUT4 intrinsic activity. *Am J Physiol Endocrinol Metab* 293: E783–E793, 2007.
- Badin PM, Louche K, Mairal A, Liebisch G, Schmitz G, Rustan AC, Smith SR, Langin D, Moro C. Altered skeletal muscle lipase expression and activity contribute to insulin. *Diabetes* 60: 1734–1742, 2011.
- Bajaj M, Baig R, Suraamornkul S, Hardies LJ, Coletta DK, Cline GW, Monroy A, Koul S, Sriwijitkamol A, Musi N, Shulman GI, DeFronzo RA. Effects of pioglitazone on intramyocellular fat metabolism in patients with type 2 diabetes mellitus. *J Clin Endocrinol Metab* 95: 1916–1923, 2010.
- Bartke N, Hannun YA. Bioactive sphingolipids: metabolism and function. *J Lipid Res* 50, Suppl: S91–S96, 2009.
- Beha A, Juretschke HP, Kuhlmann J, Neumann-Haefelin C, Belz U, Gerl M, Kramer W, Roden M, Herling AW. Muscle type-specific fatty acid metabolism in insulin resistance: an integrated in vivo study in Zucker diabetic fatty rats. *Am J Physiol Endocrinol Metab* 290: E989–E997, 2006.
- Bergouignan A, Trudel G, Simon C, Chopard A, Schoeller DA, Momken I, Votruba SB, Desage M, Burdge GC, Gauquelin-Koch G, Normand S, Blanc S. Physical inactivity differentially alters dietary oleate and palmitate trafficking. *Diabetes* 58: 367–376, 2009.
- Bionda C, Portoukalian J, Schmitt D, Rodriguez-Lafrasse C, Ardail D. Subcellular compartmentalization of ceramide metabolism: MAM (mitochondria-associated membrane) and/or mitochondria? *Biochem J* 382: 527–533, 2004.
- Blachnio-Zabielska A, Zabielski P, Baranowski M, Gorski J. Effects of streptozotocin-induced diabetes and elevation of plasma FFA on ceramide metabolism in rat skeletal muscle. *Horm Metab Res* 42: 1–7, 2010.
- Blachnio-Zabielska AU, Koutsari C, Jensen MD. Measuring long-chain acyl-coenzyme A concentrations and enrichment using liquid chromatography/tandem mass spectrometry with selected reaction monitoring. *Rapid Commun Mass Spectrom* 25: 2223–2230, 2011.
- Blachnio-Zabielska AU, Persson XM, Koutsari C, Zabielski P, Jensen MD. A liquid chromatography/tandem mass spectrometry method for measuring the in vivo incorporation of plasma free fatty acids into intramyocellular ceramides in humans. *Rapid Commun Mass Spectrom* 26: 1134–1140, 2012.
- Chavez JA, Summers SA. Characterizing the effects of saturated fatty acids on insulin signaling and ceramide and diacylglycerol accumulation in 3T3-L1 adipocytes and C2C12 myotubes. *Arch Biochem Biophys* 419: 101–109, 2003.
- Cleland SJ. Cardiovascular risk in double diabetes mellitus—when two worlds collide. In: *Nat Rev Endocrinol* 8: 476–485, 2012.
- Cnop M. Fatty acids and glucolipotoxicity in the pathogenesis of Type 2 diabetes. *Biochem Soc Trans* 36: 348–352, 2008.
- Coll T, Eyre E, Rodríguez-Calvo R, Palomer X, Sánchez RM, Merlos M, Laguna JC, Vázquez-Carrera M. Oleate reverses palmitate-induced insulin resistance and inflammation in skeletal muscle cells. *J Biol Chem* 283: 11107–11116, 2008.
- Colomiere M, Permezel M, Lappas M. Diabetes and obesity during pregnancy alter insulin signalling and glucose transporter expression in maternal skeletal muscle and subcutaneous adipose tissue. *J Mol Endocrinol* 44: 213–223, 2010.
- Davidson EP, Coppey LJ, Holmes A, Yorek MA. Effect of inhibition of angiotensin converting enzyme and/or neutral endopeptidase on vascular and neural complications in high fat fed/low dose streptozotocin-diabetic rats. *Eur J Pharmacol* 677: 180–187, 2012.
- Del Prato S, Nosadini R, Tiengo A, Tessari P, Avogaro A, Trevisan R, Valerio A, Muggeo M, Cobelli C, Toffolo G. Insulin-mediated glucose disposal in type I diabetes: evidence for insulin resistance. *J Clin Endocrinol Metab* 57: 904–910, 1983.
- Demigne C, Bloch-Faure M, Picard N, Sabboh H, Besson C, Remesy C, Geoffroy V, Gaston AT, Nicoletti A, Hagege A, Menard J, Meneton P. Mice chronically fed a westernized experimental diet as a model of obesity. *Eur J Nutr* 45: 298–306, 2006.
- Dimopoulos N, Watson M, Sakamoto K, Hundal HS. Differential effects of palmitate and palmitoleate on insulin action and glucose utilization in rat L6 skeletal muscle cells. *Biochem J* 399: 473–481, 2006.
- Dubé JJ, Amati F, Toledo FG, Stefanovic-Racic M, Rossi A, Coen P, Goodpaster BH. Effects of weight loss and exercise on insulin resistance, and intramyocellular triacylglycerol, diacylglycerol and ceramide. *Diabetologia* 54: 1147–1156, 2011.
- Ellis BA, Poynten A, Lowy AJ, Furler SM, Chisholm DJ, Kraegen EW, Cooney GJ. Long-chain acyl-CoA esters as indicators of lipid metabolism and insulin sensitivity in rat and human muscle. *Am J Physiol Endocrinol Metab* 279: E554–E560, 2000.
- Flamment M, Hajduch E, Ferre P, Foufelle F. New insights into ER stress-induced insulin resistance. *Trends Endocrinol Metab* 23: 381–390, 2012.
- Franko A, von Kleist-Retzow JC, Böse M, Sanchez-Lasheras C, Brodesser S, Krut O, Kunz WS, Wiedermann D, Hoehn M, Stöhr O, Moll L, Freude S, Krone W, Schubert M, Wiesner RJ. Complete failure of insulin-transmitted signaling, but not obesity-induced insulin resistance, impairs respiratory chain function in muscle. *J Mol Med (Berl)* 90: 1145–1160, 2012.
- Gentil B, Grimot F, Riva C. Commitment to apoptosis by ceramides depends on mitochondrial respiratory function, cytochrome c release and caspase-3 activation in Hep-G2 cells. *Mol Cell Biochem* 254: 203–210, 2003.
- Glatz JF, Bonen A, Luiken JJ. Exercise and insulin increase muscle fatty acid uptake by recruiting putative fatty acid transporters to the sarcolemma. *Curr Opin Clin Nutr Metab Care* 5: 365–370, 2002.
- Hanada K, Kumagai K, Yasuda S, Miura Y, Kawano M, Fukasawa M, Nishijima M. Molecular machinery for non-vesicular trafficking of ceramide. *Nature* 426: 803–809, 2003.

27. Haugaard SB, Madsbad S, Mu H, Vaag A. Desaturation of excess intramyocellular triacylglycerol in obesity: implications. *Int J Obes (Lond)* 34: 500–510, 2010.
28. Heart E, Choi WS, Sung CK. Glucosamine-induced insulin resistance in 3T3-L1 adipocytes. *Am J Physiol Endocrinol Metab* 278: E103–E112, 2000.
29. Holland WL, Brozinick JT, Wang LP, Hawkins ED, Sargent KM, Liu Y, Narra K, Hoehn KL, Knotts TA, Siesky A, Nelson DH, Karathanasis SK, Fontenot GK, Birnbaum MJ, Summers SA. Inhibition of ceramide synthesis ameliorates glucocorticoid-, saturated-fat-, and obesity-induced insulin resistance. *Cell Metab* 5: 167–179, 2007.
30. Issandou M, Bouillot A, Brusq JM, Forest MC, Grillot D, Guillard R, Martin S, Michiels C, Sulpice T, Daugan A. Pharmacological inhibition of stearoyl-CoA desaturase 1 improves insulin. *Eur J Pharmacol* 618: 28–36, 2009.
31. Itani SI, Ruderman NB, Schmieder F, Boden G. Lipid-induced insulin resistance in human muscle is associated with changes in diacylglycerol, protein kinase C, and IkappaB-alpha. *Diabetes* 51: 2005–2011, 2002.
32. Jensen MD, Caruso M, Heiling V, Miles JM. Insulin regulation of lipolysis in nondiabetic and IDDM subjects. *Diabetes* 38: 1595–1601, 1989.
33. Karolina DS, Armugam A, Tavintharan S, Wong MT, Lim SC, Sum CF, Jeyaseelan K. MicroRNA 144 impairs insulin signaling by inhibiting the expression of insulin receptor substrate 1 in type 2 diabetes mellitus. *PLoS One* 6: e22839, 2011.
34. Kim JK, Fillmore JJ, Chen Y, Yu C, Moore IK, Pypaert M, Lutz EP, Kako Y, Velez-Carrasco W, Goldberg IJ, Breslow JL, Shulman GI. Tissue-specific overexpression of lipoprotein lipase causes tissue-specific insulin resistance. *Proc Natl Acad Sci USA* 98: 7522–7527, 2001.
35. Kim JK, Fillmore JJ, Sunshine MJ, Albrecht B, Higashimori T, Kim DW, Liu ZX, Soos TJ, Cline GW, O'Brien WR, Littman DR, Shulman GI. PKC-theta knockout mice are protected from fat-induced insulin resistance. *J Clin Invest* 114: 823–827, 2004.
36. Kovacs P, Hanson RL, Lee YH, Yang X, Kobes S, Permana PA, Bogardus C, Baier LJ. The role of insulin receptor substrate-1 gene (IRS1) in type 2 diabetes in Pima Indians. *Diabetes* 52: 3005–3009, 2003.
37. Kuda O, Jelenik T, Jilkova Z, Flachs P, Rossmel M, Hensler M, Kazdova L, Ogston N, Baranowski M, Gorski J, Janovska P, Kus V, Polak J, Mohamed-Ali V, Burcelin R, Cinti S, Bryhn M, Kopecky J. n-3 fatty acids and rosiglitazone improve insulin sensitivity through additive stimulatory effects on muscle glycogen synthesis in mice fed a high-fat diet. *Diabetologia* 52: 941–951, 2009.
38. Lanza IR, Nair KS. Mitochondrial metabolic function assessed in vivo and in vitro. *Curr Opin Clin Nutr Metab Care* 13: 511–517, 2010.
39. Laybutt DR, Schmitz-Peiffer C, Saha AK, Ruderman NB, Biden TJ, Kraegen EW. Muscle lipid accumulation and protein kinase C activation in the insulin-resistant chronically glucose-infused rat. *Am J Physiol Endocrinol Metab* 277: E1070–E1076, 1999.
40. Lee JS, Pinnamaneni SK, Eo SJ, Cho IH, Pyo JH, Kim CK, Sinclair AJ, Febbraio MA, Watt MJ. Saturated, but not n-6 polyunsaturated, fatty acids induce insulin resistance: role of intramuscular accumulation of lipid metabolites. *J Appl Physiol* 100: 1467–1474, 2006.
41. Leguisamo NM, Lehnen AM, Machado UF, Okamoto MM, Markoski MM, Pinto GH, Schaun BD. GLUT4 content decreases along with insulin resistance and high levels of inflammatory markers in rats with metabolic syndrome. *Cardiovasc Diabetol* 11: 100, 2012.
42. Li Y, Soos TJ, Li X, Wu J, Degennaro M, Sun X, Littman DR, Birnbaum MJ, Polakiewicz RD. Protein kinase C Theta inhibits insulin signaling by phosphorylating IRS1 at Ser(1101). *J Biol Chem* 279: 45304–45307, 2004.
43. Longato L, Ripp K, Setshedi M, Dostalek M, Akhlaghi F, Branda M, Wands JR, de la Monte SM. Insulin resistance, ceramide accumulation, and endoplasmic reticulum stress in human chronic alcohol-related liver disease. *Oxid Med Cell Longev* 2012: 479348, 2012.
44. Luiken JJ, Arumugam Y, Bell RC, Calles-Escandon J, Tandon NN, Glatz JF, Bonen A. Changes in fatty acid transport and transporters are related to the severity of insulin deficiency. *Am J Physiol Endocrinol Metab* 283: E612–E621, 2002.
45. Merrill AH Jr. Sphingolipid and glycosphingolipid metabolic pathways in the era of sphingolipidomics. *Chem Rev* 111: 6387–6422, 2011.
46. Miyazaki M, Sampath H, Liu X, Flowers MT, Chu K, Dobrzyn A, Ntambi JM. Stearoyl-CoA desaturase-1 deficiency attenuates obesity and insulin resistance in leptin-resistant obese mice. *Biochem Biophys Res Commun* 380: 818–822, 2009.
47. Mokhtar N, Rousseau-Mignerot S, Tancrede G, Nadeau A. Physical training attenuates phosphocreatine and long-chain acyl-CoA alterations in diabetic rat heart. *J Appl Physiol* 74: 1785–1790, 1993.
48. Moro C, Galgani JE, Luu L, Pasarica M, Mairal A, Bajpeyi S, Schmitz G, Langin D, Liebisch G, Smith SR. Influence of gender, obesity, and muscle lipase activity on intramyocellular lipids in sedentary individuals. *J Clin Endocrinol Metab* 94: 3440–3447, 2009.
49. Mullen TD, Hannun YA, Obeid LM. Ceramide synthases at the centre of sphingolipid metabolism and biology. *Biochem J* 441: 789–802, 2012.
50. Patel SA, Hoehn KL, Lawrence RT, Sawbridge L, Talbot NA, Tomsig JL, Turner N, Cooney GJ, Whitehead JP, Kraegen EW, Cleasby ME. Overexpression of the adiponectin receptor AdipoR1 in rat skeletal muscle amplifies local insulin sensitivity. *Endocrinology* 153: 5231–5246, 2012.
51. Persson XM, Blachnio-Zabielska AU, Jensen MD. Rapid measurement of plasma free fatty acid concentration and isotopic enrichment using LC/MS. *J Lipid Res* 51: 2761–2765, 2010.
52. Pickersgill L, Litherland GJ, Greenberg AS, Walker M, Yeaman SJ. Key role for ceramides in mediating insulin resistance in human muscle cells. *J Biol Chem* 282: 12583–12589, 2007.
53. Powell DJ, Turban S, Gray A, Hajdich E, Hundal HS. Intracellular ceramide synthesis and protein kinase Czeta activation play an essential role in palmitate-induced insulin resistance in rat L6 skeletal muscle cells. *Biochem J* 382: 619–629, 2004.
54. Ramirez T, Longato L, Dostalek M, Tong M, Wands JR, de la Monte SM. Insulin resistance, ceramide accumulation and endoplasmic reticulum stress in experimental chronic alcohol-induced steatohepatitis. *Alcohol Alcohol* 48: 39–52, 2013.
55. Sabin MA, Stewart CE, Crowne EC, Turner SJ, Hunt LP, Welsh GI, Grohmann MJ, Holly JM, Shield JP. Fatty acid-induced defects in insulin signalling, in myotubes derived from children, are related to ceramide production from palmitate rather than the accumulation of intramyocellular lipid. *J Cell Physiol* 211: 244–252, 2007.
56. Salvadó L, Coll T, Gómez-Foix AM, Salmerón E, Barroso E, Palomer X, Vázquez-Carrera M. Oleate prevents saturated-fatty-acid-induced ER stress, inflammation and insulin resistance in skeletal muscle cells through an AMPK-dependent mechanism. *Diabetologia* 56: 1372–1382, 2013.
57. Samuel VT, Liu ZX, Qu X, Elder BD, Bilz S, Befroy D, Romanelli AJ, Shulman GI. Mechanism of hepatic insulin resistance in non-alcoholic fatty liver disease. *J Biol Chem* 279: 32345–32353, 2004.
58. Schmitz-Peiffer C, Browne CL, Oakes ND, Watkinson A, Chisholm DJ, Kraegen EW, Biden TJ. Alterations in the expression and cellular localization of protein kinase C. *Diabetes* 46: 169–178, 1997.
59. Schmitz-Peiffer C, Craig DL, Biden TJ. Ceramide generation is sufficient to account for the inhibition of the insulin-stimulated PKB pathway in C2C12 skeletal muscle cells pretreated with palmitate. *J Biol Chem* 274: 24202–24210, 1999.
60. Selvin E, Steffes MW, Gregg E, Brancati FL, Coresh J. Performance of A1C for the classification and prediction of diabetes. *Diabetes Care* 34: 84–89, 2011.
61. Shanik MH, Xu Y, Skrha J, Dankner R, Zick Y, Roth J. Insulin resistance and hyperinsulinemia: is hyperinsulinemia the cart or the horse? *Diabetes Care* 31, Suppl 2: S262–S268, 2008.
62. Song F, Schmidt AM. Glycation and insulin resistance: novel mechanisms and unique targets? *Arterioscler Thromb Vasc Biol* 32: 1760–1765, 2012.
63. Stein DT, Stevenson BE, Chester MW, Basit M, Daniels MB, Turley SD, McGarry JD. The insulinotropic potency of fatty acids is influenced profoundly by their chain length and degree of saturation. *J Clin Invest* 100: 398–403, 1997.
64. Storz P, Döppler H, Wernig A, Pfizenmaier K, Müller G. Cross-talk mechanisms in the development of insulin resistance of skeletal muscle cells palmitate rather than tumour necrosis factor inhibits insulin-dependent protein kinase B (PKB)/Akt stimulation and glucose uptake. *Eur J Biochem* 266: 17–25, 1999.
65. Straczkowski M, Kowalska I, Baranowski M, Nikolajuk A, Oziomek E, Zabielski P, Adamska A, Blachnio A, Gorski J, Gorska M. Increased skeletal muscle ceramide level in men at risk of developing type 2 diabetes. *Diabetologia* 50: 2366–2373, 2007.
66. Straczkowski M, Kowalska I, Nikolajuk A, Dzienis-Straczkowska S, Kinalska I, Baranowski M, Zendzian-Piotrowska M, Brzezinska Z, Gorski J. Relationship between insulin sensitivity and sphingomyelin signaling pathway in human skeletal muscle. *Diabetes* 53: 1215–1221, 2004.

67. **Tesch GH, Allen TJ.** Rodent models of streptozotocin-induced diabetic nephropathy. *Nephrology (Carlton)* 12: 261–266, 2007.
68. **Thompson AL, Cooney GJ.** Acyl-CoA inhibition of hexokinase in rat and human skeletal muscle is a potential mechanism of lipid-induced insulin resistance. *Diabetes* 49: 1761–1765, 2000.
69. **Thompson AL, Lim-Fraser MY, Kraegen EW, Cooney GJ.** Effects of individual fatty acids on glucose uptake and glycogen synthesis in soleus muscle in vitro. *Am J Physiol Endocrinol Metab* 279: E577–E584, 2000.
70. **Unger RH, Grundy S.** Hyperglycaemia as an inducer as well as a consequence of impaired islet cell function and insulin resistance: implications for the management of diabetes. *Diabetologia* 28: 119–121, 1985.
71. **Ussher JR, Koves TR, Cadete VJ, Zhang L, Jaswal JS, Swyrd SJ, Lopaschuk DG, Proctor SD, Keung W, Muoio DM, Lopaschuk GD.** Inhibition of de novo ceramide synthesis reverses diet-induced insulin resistance. *Diabetes* 59: 2453–2464, 2010.
72. **Vestergaard H, Bjørbaek C, Andersen PH, Bak JF, Pedersen O.** Impaired expression of glycogen synthase mRNA in skeletal muscle of NIDDM patients. *Diabetes* 40: 1740–1745, 1991.
73. **Vlassara H, Striker GE.** AGE restriction in diabetes mellitus: a paradigm shift. *Nat Rev Endocrinol* 7: 526–539, 2011.
74. **Wrede CE, Dickson LM, Lingohr MK, Briaud I, Rhodes CJ.** Fatty acid and phorbol ester-mediated interference of mitogenic signaling via novel protein kinase C isoforms in pancreatic beta-cells (INS-1). *J Mol Endocrinol* 30: 271–286, 2003.
75. **Yaney GC, Korchak HM, Corkey BE.** Long-chain acyl CoA regulation of protein kinase C and fatty acid potentiation of glucose-stimulated insulin secretion in clonal beta-cells. *Endocrinology* 141: 1989–1998, 2000.
76. **Yano M, Watanabe K, Yamamoto T, Ikeda K, Senokuchi T, Lu M, Kadomatsu T, Tsukano H, Ikawa M, Okabe M, Yamaoka S, Okazaki T, Umehara H, Gotoh T, Song WJ, Node K, Taguchi R, Yamagata K, Oike Y.** Mitochondrial dysfunction and increased reactive oxygen species impair insulin secretion in sphingomyelin synthase 1-null mice. *J Biol Chem* 286: 3992–4002, 2011.
77. **Yu C, Chen Y, Cline GW, Zhang D, Zong H, Wang Y, Bergeron R, Kim JK, Cushman SW, Cooney GJ, Atcheson B, White MF, Kraegen EW, Shulman GI.** Mechanism by which fatty acids inhibit insulin activation of insulin receptor substrate-1 (IRS-1)-associated phosphatidylinositol 3-kinase activity in muscle. *J Biol Chem* 277: 50230–50236, 2002.
78. **Yuzefovych LV, Musiyenko SI, Wilson GL, Rachek LI.** Mitochondrial DNA damage and dysfunction, and oxidative stress are associated with endoplasmic reticulum stress, protein degradation and apoptosis in high fat diet-induced insulin resistance mice. *PLoS One* 8: e54059, 2013.
79. **Zhang YC, Pileggi A, Agarwal A, Molano RD, Powers M, Brusko T, Wasserfall C, Goudy K, Zahr E, Poggioli R, Scott-Jorgensen M, Campbell-Thompson M, Crawford JM, Nick H, Flotte T, Ellis TM, Ricordi C, Inverardi L, Atkinson MA.** Adeno-associated virus-mediated IL-10 gene therapy inhibits diabetes recurrence in syngeneic islet cell transplantation of NOD mice. *Diabetes* 52: 708–716, 2003.
80. **Zong H, Wang CC, Vaitheesvaran B, Kurland IJ, Hong W, Pessin JE.** Enhanced energy expenditure, glucose utilization, and insulin sensitivity in VAMP8 null mice. *Diabetes* 60: 30–38, 2011.

